Since January 2020 Elsevier has created a COVID-19 resource centre with free information in English and Mandarin on the novel coronavirus COVID-19. The COVID-19 resource centre is hosted on Elsevier Connect, the company's public news and information website.

Elsevier hereby grants permission to make all its COVID-19-related research that is available on the COVID-19 resource centre - including this research content - immediately available in PubMed Central and other publicly funded repositories, such as the WHO COVID database with rights for unrestricted research re-use and analyses in any form or by any means with acknowledgement of the original source. These permissions are granted for free by Elsevier for as long as the COVID-19 resource centre remains active.

Biosensors and Bioelectronics 236 (2023) 115421

Contents lists available at ScienceDirect

Biosensors and Bioelectronics

journal homepage: www.elsevier.com/locate/bios

Localized surface plasmon resonance biosensor chip surface modification and signal amplifications toward rapid and sensitive detection of COVID-19 infections

Xingkai Hao [a], Jean-Philippe St-Pierre [a], Shan Zou [b], Xudong Cao [a,*]

[a] Department of Chemical and Biological Engineering, University of Ottawa, 161 Louis Pasteur, Ottawa, Ontario, K1N 6N5, Canada
[b] Metrology Research Centre, National Research Council Canada, 100 Sussex Drive, Ottawa, Ontario, K1A 0R6, Canada

ARTICLE INFO

Keywords:
Aptamers
Dendrimers
SARS-CoV-2 detection
Rolling circle amplification
Nonfouling
Surface modifications

ABSTRACT

We developed a multi-pronged approach to enhance the detection sensitivity of localized surface plasmon resonance (LSPR) sensor chips to detect SARS-CoV-2. To this end, poly(amidoamine) dendrimers were immobilized onto the surface of LSPR sensor chips to serve as templates to further conjugate aptamers specific for SARS-CoV-2. The immobilized dendrimers were shown to reduce surface nonspecific adsorptions and increase capturing ligand density on the sensor chips, thereby improving detection sensitivity. To characterize the detection sensitivity of the surface-modified sensor chips, SARS-CoV-2 spike protein receptor-binding domain was detected using LSPR sensor chips with different surface modifications. The results showed that the dendrimer-aptamer modified LSPR sensor chip exhibited a limit of detection (LOD) of 21.9 pM, a sensitivity that was 9 times and 152 times more sensitive than the traditional aptamer- or antibody-based LSPR sensor chips, respectively. In addition, detection sensitivity was further improved by combining rolling circle amplification product and gold nanoparticles to further amplify the detection signals by increasing both the target mass and plasmonic coupling effects. Using pseudo SARS-CoV-2 viral particles as detection targets, we demonstrated that this combined signal intensification approach further enhanced the detection sensitivity by 10 folds with a remarkable LOD of 148 vp/mL, making it one of the most sensitive SARS-CoV-2 detection assays reported to date. These results highlight the potential of a novel LSPR-based detection platform for sensitive and rapid detection of COVID-19 infections, as well as other viral infections and point-of-care applications.

1. Introduction

The current COVID-19 pandemic has caused millions of deaths and affected economies around the world, highlighting the need for improved technological preparedness for the next pandemic. During the COVID-19 pandemic, many biosensors (Qiu et al., 2020; Raziq et al., 2021) have been developed for the rapid detection of COVID-19 infections; however, these rapid detection biosensors suffer from various drawbacks, such as low detection sensitivities or complicated sample pre-treatments (Cennamo et al., 2021a; Tian et al., 2020), severely limiting their application as reliable alternatives to polymerase chain reaction (PCR) tests.

Localized surface plasmon resonance (LSPR) is an optical phenomenon generated by collective electron charge oscillations in metallic nanoparticles excited by a light source (Schasfoort, 2017). These charge oscillations create a highly localized evanescent field extending from the surface of the nanoparticles, which is highly sensitive to minute local variations, such as surface mass changes due to molecular binding (Schasfoort, 2017). As such, LSPR-based biosensors have been widely used in many real-time and label-free detection applications (Cennamo et al., 2021b; Lewis et al., 2021). In fact, several LSPR biosensors have already been developed to detect COVID-19-related biological targets, including nucleic acids, antibodies, proteins, and whole viral particles (Huang et al., 2021; Lewis et al., 2021; Qiu et al., 2020). While these LSPR-based methods have demonstrated good detection performances, there is still a need to further improve the sensitivity of these LSPR biosensors in order to approach that achieved by PCR-based methods (Samson et al., 2020).

To improve the detection sensitivity of LSPR biosensors, two critically important considerations – non-fouling properties of the sensor

* Corresponding author.
E-mail address: xcao@eng.uottawa.ca (X. Cao).

https://doi.org/10.1016/j.bios.2023.115421
Received 16 February 2023; Received in revised form 1 May 2023; Accepted 22 May 2023
Available online 23 May 2023
0956-5663/© 2023 Elsevier B.V. All rights reserved.

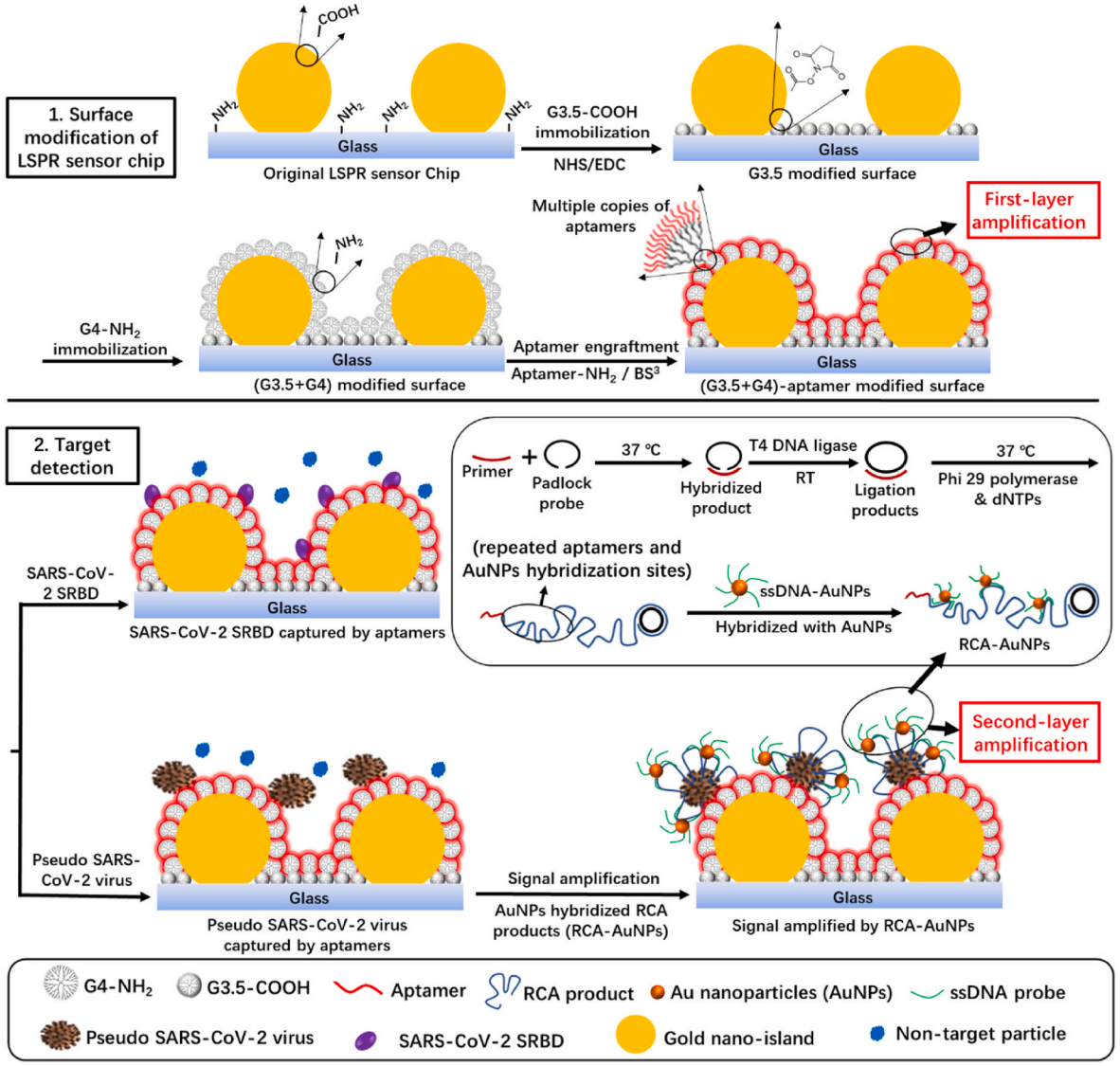

Fig. 1. Schematic illustration showing the general approach to prepare (G3.5+G4)-aptamer modified LSPR sensor chips for sensitive detection of the SARS-CoV-2 SRBD and SARS-CoV-2 pseudo viral particles. Note that the second-layer amplification is only possible with SARS-CoV-2 pseudo viral particles as the detection targets upon which the detection sandwich format can be built.

chip surfaces and high surface-ligand densities on the sensor chip surfaces – must be simultaneously targeted and integrated into the sensor chip designs (Hao et al. 2023a, 2023b). For example, it is crucial for the sensor chip surfaces to minimize nonspecific adsorptions, thereby decreasing the background noises and ultimately enhancing the signal-to-noise ratio and thus detection sensitivity (Hao et al. 2023a, 2023b). Furthermore, sensor chip surfaces with increased detection ligand density could lead to a higher probability of target capture and stronger binding avidity (Wang et al., 2022), thus resulting in higher detection sensitivity.

Aptamers are a special type of single-stranded DNA or RNA oligonucleotides – selected through a cyclic process known as systematic evolution of ligands by exponential enrichment (SELEX) from DNA/RNA libraries of random sequences – that can recognize specific targets, such as proteins, toxins, and cells (Tuerk and Gold, 1990). Recently, Song et al. selected an aptamer specifically targeting the SARS-CoV-2 spike protein receptor-binding domain (SRBD) with a high binding affinity (Kd = 5.8 nM) and specificity (Song et al., 2020). This aptamer has been widely used in different biosensors for SARS-CoV-2 detections (Amouzadeh Tabrizi and Acedo, 2022; Jiang et al., 2022; Xue et al., 2022), and it is also used in the current study.

Poly(amidoamine) (PAMAM) dendrimers are hyper-branched polymers that can be synthesized to feature a range of different surface functional groups, including -OH, -COOH, and $–NH_2$. Because of their unique structure, PAMAM dendrimers have been used as multi-handled templates via which capturing ligands, such as aptamers and antibodies, can be conjugated onto capturing surfaces to allow for enhanced target capturing probability and binding avidity for improved detection performance (Wang et al., 2022). In addition, immobilization of PAMAM dendrimers onto the detection surfaces can render the resulting surface nonfouling to minimize background noises (Hao et al. 2023a, 2023b).

Rolling circle amplification (RCA) reactions can generate long single-stranded DNA molecules with hundreds or thousands of tandem repeating units from a circular template, the nucleotide sequence of which can be designed to either capture specific targets, amplify signals, or do both (He et al., 2014). With these repeating units, the RCA products can be used to hybridize with a large amount of ssDNA functionalized gold nanoparticles (*i.e.,* ssDNA-AuNPs) to form RCA-gold nanoparticle complexes (RCA-AuNPs) that are known to intensify LSPR detection signals due to both significantly improved target mass and plasmonic coupling effect (He et al., 2014; Kim et al., 2022; Xiang et al., 2013). For example, the RCA-AuNPs have been applied to conjugate

with surface-captured targets on a surface plasmon resonance (SPR) sensor chip to improve detection signals (He et al., 2014).

In this study, we report our most recent efforts to enhance the detection sensitivity of regular LSPR sensor chips – prepared using a widely employed gold nanoislands/poly (allylamine hydrochloride) (PAH)/poly(sodium 4-styrenesulfonate) (PSS) method (Lu et al., 2021) – by implementing a multi-pronged design that aims to both reduce background noises and enhance detection signals. To reduce the background noises, both the exposed glass surfaces and gold nanoislands of the sensor chip are modified with PAMAM dendrimers to render them nonfouling and prevent non-target molecules and particles from adsorbing to the sensor chip surfaces. To enhance the detection signals, the following strategies are explored: a) an increased density of capturing aptamers specific for the targets are immobilized onto the sensor chip detection surfaces via the multi-handled PAMAM dendrimers, resulting in higher capturing probability and binding avidity for target recognition and capture (*i.e.,* first-layer amplification); and b) RCA-AuNPs complexes that incorporate both a large number of AuNPs and tandem repeating aptamers specific for the targets are employed to bind to surface captured targets (*i.e.,* SARS-CoV-2 pseudo viral particles) in a sandwich detection format to improve detection signals (*i.e.,* second-layer amplification) by both (1) increasing the target mass (from both RCA products and AuNPs) and (2) improving plasmonic coupling effect (from the AuNPs) (He et al., 2014; Kim et al., 2022). The performances of these PAMAM dendrimer-aptamer modified sensor chips are evaluated using both the SARS-CoV-2 SRBD and SARS-CoV-2 pseudo viral particles. Our results show that the modified sensor chip is 152 times more sensitive than the antibody-immobilized sensor chip (traditional method) in detecting SRBD samples (*i.e.,* due to first-layer amplification). Application of RCA-AuNPs signal amplification results in an additional 10-time improvement in the detection signal intensity when detecting SARS-CoV-2 pseudo viral particles (*i.e.,* due to second-layer amplification). With this two-layered signal amplification approach, we report a LOD of 148 viral particles per milliliter (vp/mL), one of the highest sensitivities reported in whole viral particle detections amongst all detection platforms (Huang et al., 2021; Nguyen et al., 2016; Park et al., 2014; Yang et al., 2022), making it sufficiently sensitive for the diagnosis of early COVID-19 infections (Huang et al., 2021).

2. Material and methods

2.1. Overall design

As illustrated in Fig. 1, LSPR sensor chip surfaces are modified sequentially with generation 3.5 carboxylated PAMAM dendrimers (*i.e.,* G3.5-COOH) and generation 4 aminated PAMAM dendrimers (*i.e.,* G4-NH_2) to render the resulting surfaces nonfouling. The immobilized G4 dendrimers act as multi-handled templates to allow for subsequent conjugation of numerous copies of aptamers specific for binding of SARS-CoV-2 SRBD (Song et al., 2020) (first-layer amplification). The resulting sensor chips are used to detect COVID-19 targets (*i.e.,* either SARS-CoV-2 SRBD or SARS-CoV-2 pseudo viral particles presenting spike proteins on the viral particle surfaces). For the case of SARS-CoV-2 pseudo viral particle detection, RCA-AuNPs are also employed to bind with the surface-captured viral particles and to further amplify the detection signal by increasing the target mass and plasmonic coupling effect (second-layer amplification).

2.2. Materials

Detailed information on chemicals and pseudo-SARS-CoV-2 viral particles for this study are provided in S1.1 in Supporting Information (SI); gold nanoislands (diameter = 100 nm)/PAH/PSS LSPR sensor chips with carboxyl functionalization on gold nanoislands were prepared as detailed in S1.2 (SI). Details of DNA sequences used for this study are listed below:

Capturing aptamer (*i.e.,* aptamer specific for binding of SARS-CoV-2 SRBD) (Song et al., 2020):

NH_2, 12C spacer-CAG CAC CGA CCT TGT GCT TTG GGA GTG CTG GTC CAA GGG CGT TAA TGG ACA.

RCA primer:

GGA CAT TTT TTT TTT TTT TTT CAG CA.

RCA padlock probe:

Phos-AAA AAA AAT GTC CAT TAA CGC CCT TGG ACC AGC ACT CCC AAA GCA CAA GGT CGG TGC TGA AAA AAA A-3

ssDNA probe:

Thio, 6C spacer-AAA AAA AAA AAA AAA A.

Note: The underlined portion in the RCA padlock probe sequence is complementary to the sequence of capturing aptamer in order to produce tandem repeating aptamer by the RCA reaction. The ssDNA probe is complementary to the sequence of the RCA product using a circular template, a conjugation product of RCA primer and padlock probe.

2.3. LSPR measurements

LSPR response graphs were measured using a Nicoya OpenSPR instrument (Kitchener, ON). The response graphs provide real-time tracking of the shift of peak absorbance wavelength of light absorbed by the gold nanoislands on the LSPR sensor chip as an LSPR signal in response units (RU) units (y-axis) *vs.* time (x-axis). Specifically, 1 RU equals to a 1 p.m. shift of the peak absorbance wavelength.

2.4. Surface modifications using PAMAM dendrimers and aptamers

Surface modification of the LSPR sensor chips followed the general steps outlined in Fig. 1. Since the exposed glass areas of the original LSPR sensor chip presented -NH_2 functional groups while the gold nanoislands presented -COOH groups (S2.1, SI), the sensor chip surface was first reacted with G3.5-COOH using N-hydroxysuccinimide/N-ethyl-N′-(3-(dimethylamino)propyl) carbodiimide (NHS/EDC) chemistry to immobilize G3.5-COOH on the glass areas and to convert the carboxyl surface functional groups on both the glass areas and the gold nanoislands to NHS esters (Hermanson, 2013). Specifically, the LSPR sensor chips were loaded into the Nicoya OpenSPR instrument to form a microfluidic channel based LSPR biosensor, after which a G3.5-COOH immobilization solution, including 50 μM G3.5-COOH, 0.1 M NHS, and 0.1 M EDC in PBS (pH 7.4), was injected into the channel to react with the LSPR sensor chip surfaces at a flow rate of 10 μL/min for 10 min. Subsequently, the resulting sensor chip was carefully rinsed with PBS (pH 7.4) at a flow rate of 10 μL/min until the signal baseline was stabilized.

Subsequently, G4-NH_2 was immediately immobilized onto the surfaces of the LSPR sensor chip via the NHS-esters obtained during the previous step. Briefly, a 100 μM G4-NH_2 in PBS (pH 7.4) was injected into the channel to react with the G3.5 modified LSPR sensor chip at a flow rate of 10 μL/min for 10 min, after which the G4 immobilized chip was rinsed with PBS (pH 7.4) at a flow rate of 10 μL/min until the signal baseline was stabilized. In this modification step, the G4-NH_2 molecules were immobilized onto both the gold nanoislands and the immobilized G3.5 molecules. It is important that G4-NH_2 immobilization should be conducted immediately after the G3.5-COOH modification, as NHS-esters are known to be readily hydrolyzed (Hermanson, 2013). The immobilized G4-NH_2 molecules were used as multi-handled templates to provide multiple binding sites (*i.e.,* -NH_2 groups) in the next step to further conjugate aptamers.

Finally, to conjugate amino-capped aptamers (*i.e.,* NH_2-aptamer, specific for SRBD) onto the sensor chip surfaces via the immobilized G4-NH_2 templates, a widely used bis(sulfosuccinimidyl)suberate (BS^3) crosslinker was employed (Staros, 1982). As the BS^3 crosslinker contains homobifunctional sulfo-NHS-esters that can efficiently conjugate molecules containing primary amino groups (Staros, 1982), the aptamer-NH_2 can be readily conjugated with the surface immobilized G4-NH_2

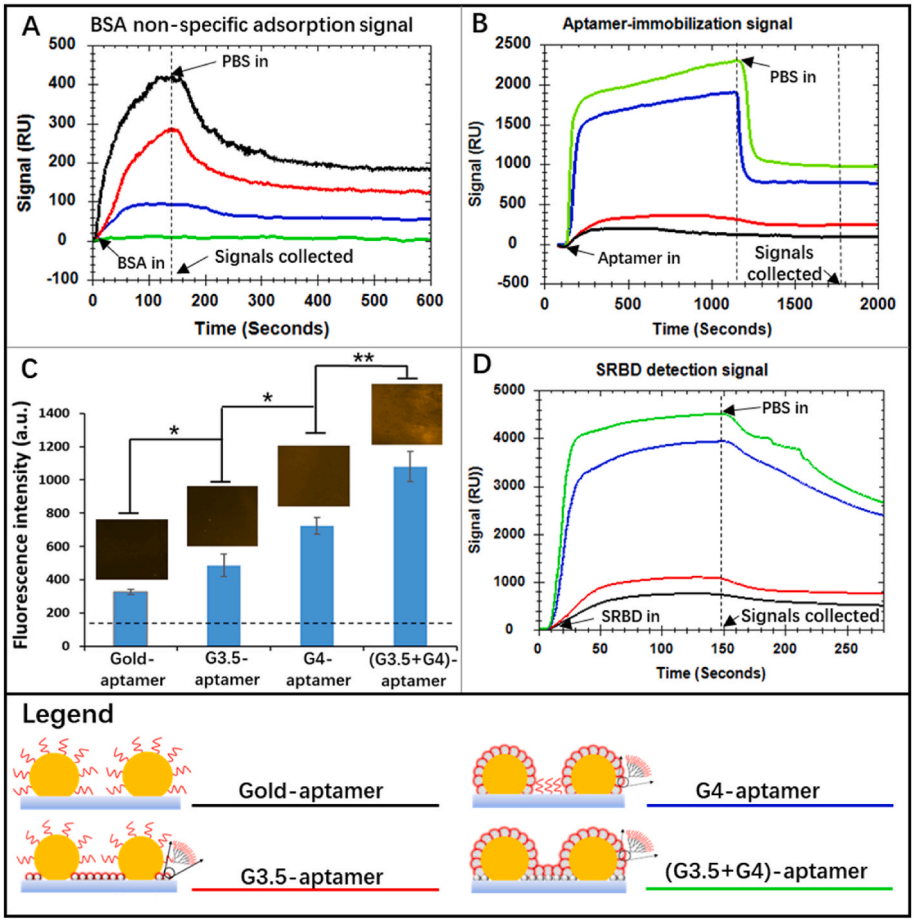

Fig. 2. LSPR sensorgraphs of different tests to evaluate performances of different sensor chip surface modifications. A) Detection background noises of different sensor chips as evaluated in a nonspecific adsorption experiment using BSA (1 mg/mL). B) Comparison of the amount of aptamers immobilized on the surface of gold nanoislands of different sensor chips. C) Comparisons of the relative amount of aptamers immobilized on the surfaces of different sensor chips as indicated by the fluorescence intensity of the surface-immobilized fluorescently labeled aptamers; the dotted line indicates fluorescence intensity of original sensor chips (*i.e.,*144.2 ± 8.2 a.u. (n = 3)); and error bars indicate standard deviation, n = 3, the *p* values (*<0.05, **<0.01) were calculated by a Student's t-test, 2 tails. D) Detection signals of SRBD (377.36 nM) on different modified surfaces. Note: all except the (G3.5+G4)-aptamer in Fig. 2D were blocked by BSA before SRBD testing. Legends signify surfaces with different modification strategies, including gold-aptamer (black curve), G3.5-aptamer (red), G4-aptamer (blue), and (G3.5+G4)-aptamer (green) for all tests.

molecules acting as templates. In a typical reaction, an aptamer conjugation solution containing 200 μM aptamers and 20 mM BS^3 in PBS (pH 7.4) was injected into the (G3.5+G4) modified LSPR sensor chip at a flow rate of 5 μL/min for 20 min to conjugate aptamers onto the G3.5+G4 templated surface. Subsequently, an ethanolamine-HCL solution (1 M, pH 8.5) was injected into the modified LSPR sensor chip at a flow rate of 20 μL/min for 5 min to deactivate the reaction, after which the sensor chip was carefully rinsed with PBS (pH 7.4) at a flow rate of 30 μL/min until the signal baseline was stabilized.

2.5. Preparation of RCA-AuNPs

To prepare RCA-AuNPs, ssDNA-AuNPs and RCA products were first individually synthesized. Specifically, to obtain ssDNA-AuNPs, a well-established protocol that involved the reduction of $HAuCl_4$ by trisodium citrate was followed (Frens, 1973); subsequently, the obtained AuNPs were used to conjugate ssDNA probes as demonstrated in a previous study (Hurst et al., 2006). To synthesize the RCA product, a previously published RCA reaction protocol was followed with minor modifications (Jiang et al., 2019; Li et al., 2021). Specifically, 100 μL of 1 μM circular template was first prepared using T4 DNA ligase to ligate hybridization RCA primer and padlock probe. Subsequently, the prepared circular template solution was mixed with an RCA reaction mixture, including 10 μL of phi29 DNA polymerase (10 U/μL), 40 μL of dNTP (10 mM), 100 μL of 10 × phi29 polymerase buffer, and 750 μL of nuclease-free water, to react at 37 °C for 1 h to obtain RCA products. The RCA reaction was stopped by heating at 65 °C for 10 min to inactivate the phi29 DNA polymerase.

To synthesize the RCA-AuNPs complex, RCA products obtained from the previous step were mixed with 1 mL of ssDNA-AuNPs, after which the reaction mixture was treated in 95 °C for 10 min, quickly cooled in an ice bath for 1 min, and subsequently incubated at 37 °C for 30 min to allow hybridization between RCA products and ssDNA-AuNPs conjugates. Finally, the resulting solution was centrifuged for 20 min at 8000×*g*, and the ssDNA-AuNPs complex was collected at the bottom of the centrifuge tube. The RCA-AuNPs complex was resuspended in PBS (pH 7.4) and washed three times.

2.6. Evaluation of detection performances using SRBD samples

To evaluate the detection performances of the (G3.5+G4)-aptamer modified LSPR sensor chips, the SARS-CoV-2 SRBD was employed. Briefly, SRBD samples of different concentrations were separately injected into the (G3.5+G4)-aptamer modified LSPR sensor chip at a flow rate of 30 μL/min for 3.3 min, after which the sensor chip was regenerated using a regeneration buffer (*i.e.,* glycine-HCL (10 mM, pH 2.0) at a flow rate of 150 μL/min for 0.67 min so that the sensor chip could be regenerated (Zhao et al., 2014).

2.7. Detection of SARS-CoV-2 pseudo viral particles with RCA-AuNPs signal amplifications

To evaluate the real-world sample detection performances of the newly developed sensor chips, pseudo SARS-CoV-2 viral particles were used as detection targets; in addition, the detection signals were subsequently intensified using an *in situ* amplification step based on RCA-AuNPs complexes. Specifically, different concentrations of pseudo viral particle suspensions were separately injected into the (G3.5+G4)-aptamer modified LSPR sensor chip at a flow rate of 30 μL/min for 3.3 min, after which the sensor chip was carefully rinsed using PBS (pH 7.4)

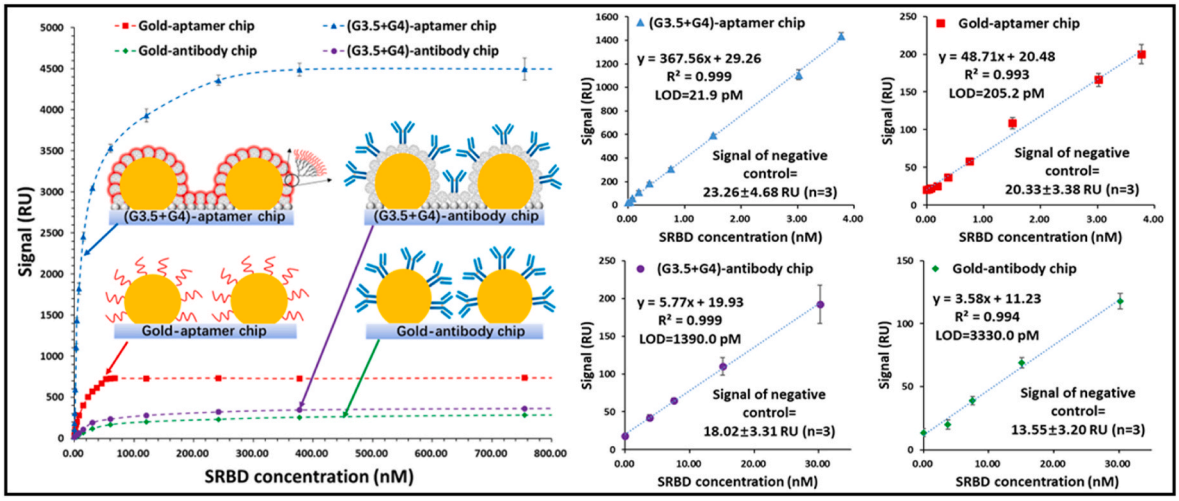

Fig. 3. Detection performances of different modified sensor chips over a wide range of SRBD concentrations; insets show linear regions of the response curves, LOD, and signal of negative controls; error bars indicate standard deviations, n = 3. Note: in obtaining the response curve, all detection parameters were optimized (S3, SI), and the gold-aptamer and gold-antibody sensor chips were properly blocked using BSA; the LSPR sensorgraphs for creating these concentration-response curves are shown in S6 (SI).

at a flow rate of 30 μL/min until the signal baseline was stabilized. Subsequently, the detection signal was amplified *in situ* based on RCA-AuNPs complexes using either a one-step or two-step amplification format. For the one-step amplification format, the RCA-AuNPs complexes were directly injected into the sensor chip at a flow rate of 30 μL/min for 3.3 min. For the two-step amplification format, RCA products were first injected into the sensor chip at a flow rate of 30 μL/min for 3.3 min, after which ssDNA-AuNPs were injected into the sensor chip again at a flow rate of 30 μL/min for another 3.3 min. To regenerate the sensor chip, the LSPR sensor chip channel was washed using a regeneration buffer at a flow rate of 150 μL/min for 0.67 min to release the captured viral particles (Zhao et al., 2014). *Caution: all experiments involving SARS-CoV-2 pseudo viral particles were carried out in a certified Risk Group II (RG II, Public Health Agency of Canada) laboratory*.

3. Results and discussion

3.1. Characterization

Characterization results are detailed in SI, including characterization of carboxyl functionalized LSPR sensor chips (S2.1), (G3.5+G4)-aptamer surface modifications (S2.2), AuNPs and ssDNA-AuNPs conjugates (S2.3), and RCA products (S2.4).

3.2. Detection performance of (G3.5+G4)-aptamer sensor chip

The ability of sensor chip surfaces to prevent nonspecific adsorption of molecules is a critical consideration for enhancing LSPR sensor sensitivity (Lichtenberg et al., 2019); therefore, the nonfouling property of the modified sensor chips was investigated by evaluating the detection background noises generated by incubation with 1 mg/mL bovine serum albumin (BSA) as a nonspecific molecule. Specifically, four different sensor chips with different surface modification configurations (see Legend of Fig. 2), namely (1) the original sensor chips functionalized directly with aptamers (*i.e.,* gold-aptamer, black curve), (2) the sensor chips with G3.5 modification on glass areas in-between the gold nanoislands and functionalized with aptamers (*i.e.,* G3.5-aptamer, red curve), (3) the sensor chips with G4 modification on the gold nanoislands and functionalized with aptamers (*i.e.,* G4-aptamer, blue curve), and (4) the sensor chips with both G3.5 and G4 modifications and functionalized with aptamers (*i.e.,* (G3.5+G4)-aptamer, green curve) were tested. As shown in Fig. 2A, gold-aptamer modified (*i.e.,* no dendrimers) sensor chips showed the highest background noises, indicating the highest amount of nonspecific surface adsorption; in contrast, the (G3.5+G4)-aptamer modified sensor chips exhibited the lowest background noises, suggesting excellent nonfouling properties of the modified surfaces. As expected, both the G3.5- and G4-aptamer modified sensor chips demonstrated significantly improved nonfouling properties compared to the gold-aptamer modified surfaces (*i.e.,* no dendrimer immobilization on the sensor chip surface), as the background noises of these sensor chips were substantially lower than those of the gold-aptamer modified. This observation suggests that nonspecific adsorption occurs on both gold nanoislands and areas between the nanoislands and that the combined immobilization of G3.5 and G4 molecules can effectively prevent nonspecific adsorptions in both areas. It was noted that the background noise of the G3.5-aptamer surface was higher than that of the G4-aptamer surface (300 *vs.* 100 RU). This is most likely because the nonspecific adsorptions on/near the gold nanoislands (*i.e.,* within the electromagnetic fields) contributed more to affecting the LSPR signals (Unser et al., 2015), further suggesting the importance of G4 immobilization on the surface of gold nanoislands. This significant improvement in nonfouling properties of the sensor chip surfaces – as a result of functionalizing the sensor chip surface with a layer of dendrimers using combined (G3.5+G4) surface modifications – results in significantly reduced background noises, thus potentially improving the detection performance of the LSPR sensor chips by enhancing the signal-to-noise ratio (Hao et al. 2023a, 2023b). It is worthwhile mentioning that the excellent nonfouling properties of the dendrimer-modified sensor chip eliminate the need for both blocking agents and reference channels specifically designed to reduce and compensate for surface nonspecific bindings in the LSPR assays, respectively (Lewis et al., 2021).

As the number of surface immobilized detection ligands (*i.e.,* aptamers) is one of the most critical considerations affecting the detection sensitivity of biosensors (Hao et al. 2023a, 2023b), we studied the relative amount of aptamers immobilized on the surface of gold nanoislands of different modified sensor chips (*i.e.,* gold-aptamer, G3.5-aptamer, G4-aptamer, and (G3.5+G4)-aptamer surfaces) by directly evaluating the LSPR sensorgraph signal changes before and after aptamer immobilizations. As shown in Fig. 2B, the gold-aptamer surface showed the lowest signal, suggesting the lowest amount of immobilized aptamers, likely due to a limited number of aptamer binding sites on the gold-nanoislands. In contrast, the (G3.5+G4)-aptamer sensor chip surface exhibited the highest aptamer immobilization signal,

approximately 10 times higher than that of the gold-aptamer surface. This significant increase of immobilized aptamers amount was most likely caused by the presence of multi-handled G4 dendrimer templates (*i.e.,* 64 binding sites per G4 molecule) via which the aptamers were immobilized on the surface of gold nanoislands. In addition, fluorescently labeled (*i.e.,* cy3) aptamers were used to conjugate to the four differently modified sensor chips in order to compare the relative amount of the aptamer amount on the complete sensor chip surfaces by comparing the fluorescence intensities of each sensor chip. As shown in Fig. 2C, the fluorescence intensity of the (G3.5+G4)-aptamer surface was significantly higher than any other surfaces investigated ($p<0.01$). Therefore, it can be concluded that the (G3.5+G4) surface-modification configuration allows for the largest amount of aptamers to be tethered on the sensor chip capturing surfaces in this study.

Furthermore, to evaluate the performance of the four modified sensor chips (*i.e.,* gold-aptamer, G3.5-aptamer, G4-aptamer, and (G3.5+G4)-aptamer surfaces), SRBD detection was carried out. For this study, the gold-aptamer, G3.5-aptamer, and G4-aptamer sensors were blocked with BSA prior to SRBD detection, while this blocking step was not performed for (G3.5+G4)-aptamer sensor chips. As shown in Fig. 2D, the detection signals from all 4 sensor chips showed patterns and trends similar to that of the gold nanoisland surface-immobilized aptamer signals seen in Fig. 2B. Specifically, the (G3.5+G4)-aptamer sensor chip showed the highest detection signal of 4490 RU, while detection signals from other sensor chips were 735 RU (gold-aptamer surface), 1080 RU (G3.5-aptamer surface), and 3900 RU (G4-aptamer surface), respectively. These results strongly indicate that the (G3.5+G4) surface modification on the sensor chip is the most effective design in conjugating a higher density of aptamers to the capturing surface, which results in an improved detection signal in comparison with other sensor chip modification approaches investigated in this study.

To further investigate the detection performances of the (G3.5+G4)-aptamer sensor chips, the sensor chips were used to detect different concentrations of SRBD samples. The same samples were also assayed using gold-aptamer, gold-antibody (*i.e.,* antibodies against SRBD), and (G3.5+G4)-antibody modified sensor chips for comparisons. As shown in Fig. 3, the (G3.5+G4)-aptamer modified sensor chips showed the highest detection signal at any given SRBD concentration assayed amongst all sensor chips investigated, including gold-aptamer, gold-antibody, and (G3.5+G4)-antibody modified surfaces. In addition, it is worth noting that the (G3.5+G4)-aptamer modified sensor chips demonstrated a much broader detection range (0.04 nM to 377.36 nM) than the gold-aptamer modified sensor chips (0.19 nM to 60.38 nM). This significantly increased detection range exhibited by the (G3.5+G4)-aptamer modified sensor chips was most likely caused by the presence of a greater amount of capturing aptamers on the (G3.5+G4) modified surface than on the non-modified sensor chips, thereby providing more target capturing capacity by allowing both more binding sites for target capturing and stronger binding avidity (Wang et al., 2022). Furthermore, the slope of the linear region of the response curve for the (G3.5+G4)-aptamer modified sensor chips (k = 367.56) was significantly greater ($p<0.05$) than those for the gold-aptamer (k = 48.71), gold-antibody (k = 3.58) and (G3.5+G4)-antibody (k = 5.77) modified sensor chips, suggesting a much higher detection sensitivity by the (G3.5+G4)-aptamer modified sensor chips (Hao et al. 2023a, 2023b).

The limit of detection, defined as the lowest target concentration to provide a signal at least three standard deviations greater than the signal from a negative control (Hao et al. 2023a, 2023b), was also calculated for each type of sensor chip. The results showed that the LOD of the (G3.5+G4)-aptamer modified sensor chip was 21.9 pM, which was around 9-time more sensitive than that of the gold-aptamer (205.2 pM) and 152-time more sensitive than that of the gold-antibody (3330.0 pM) modified sensor chip, respectively. In addition, a comparison between the (G3.5+G4)-*antibody* and the (G3.5+G4)-*aptamer* modified sensor chips reveals that the LOD of the (G3.5+G4)-*antibody* sensor chip was

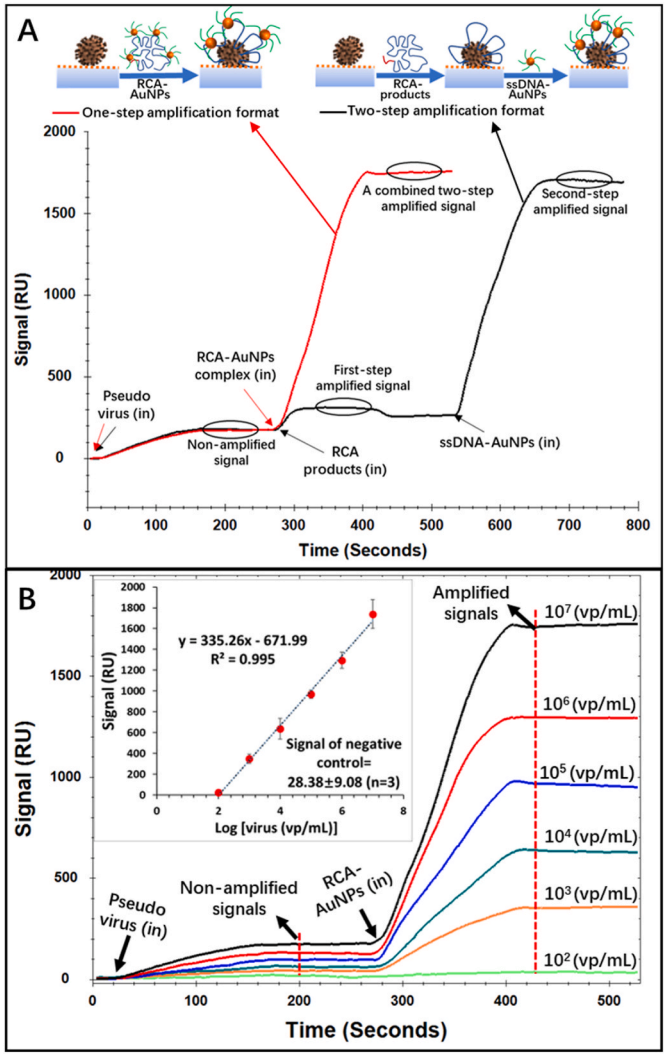

Fig. 4. Detection of SARS-CoV-2 pseudo viral particles with RCA-AuNPs signal amplification. A) LSPR sensorgarphs of one- and two-step amplification formats for signal amplification of SARS-CoV-2 pseudo viral particles (10^7 vp/mL); and B) the LSPR sensorgraph of detection of SARS-CoV-2 pseudo viral particles with RCA-AuNPs signal amplification; inset shows the relationship between the signals and the target concentrations as well as signal of the negative control; error bars indicate standard deviations, n = 3.

much higher (*i.e.,* 1390.0 pM vs. 21.9 pM). This difference is likely due to a significantly lower amount of antibodies conjugated onto the sensor chip surfaces via the G3.5+G4 templates than aptamers, resulting in less capturing ligands on the sensor detection surfaces. Indeed, aptamers are much smaller molecules than antibodies (1 nm *vs.* 10 nm) (Hao et al., 2023b); this significant differences in sizes would allow more copies of aptamers to be conjugated to the sensor chip surfaces via the G3.5+G4 templates (size 4.5 nm) than their antibodies counterparts. In fact, we estimated the number of aptamers *vs.* antibodies on the (G3.5+G4) modified surfaces as reported elsewhere (De Feijter et al., 1978; Unser et al., 2015) (see details in S5, SI). The result showed that the number of immobilized surface aptamers was 16 to 44 times greater than that of the immobilized antibodies.

3.3. Detection of SARS-CoV-2 pseudo viral particles with RCA-AuNPs signal amplification (second-layer amplification)

To further study the detection performance of the (G3.5+G4)-aptamer sensor chips, we tested SARS-CoV-2 pseudo viral particles as

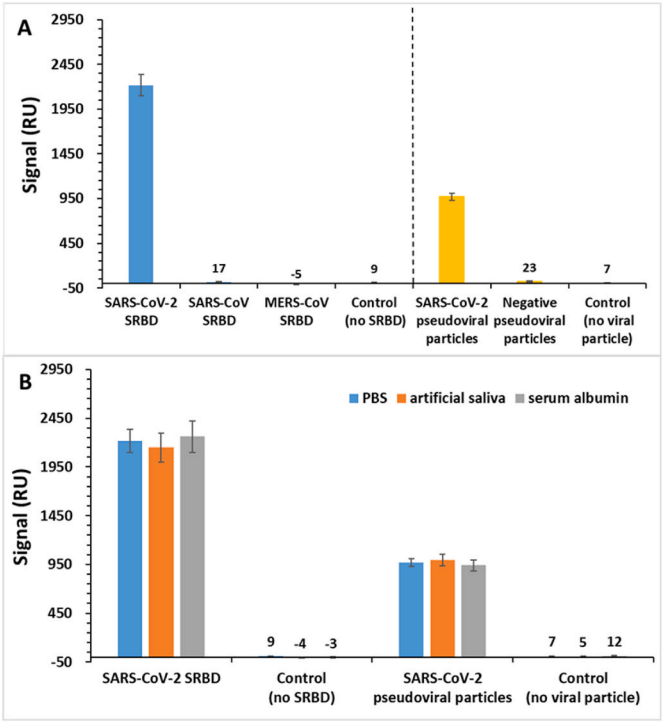

Fig. 5. Detection specificity and influence of sample matrices. A) The detection specificity of the (G3.5+G4)-aptamer modified LSPR sensor chip; the targets are SARS-CoV-2 SRBD and SARS-CoV-2 pseudo viral particles, and nonspecific targets are SARS-CoV SRBD, MERS-CoV SRBD, and negative pseudo viral particles; all SRBD samples (blue bars) were tested at 12 nM in PBS (pH 7.4), and all pseudo viral particle samples (yellow bars) were tested at 10^5 vp/mL in PBS (pH 7.4). B) Influence of sample matrices on detection performances; the SARS-CoV-2 SRBD were tested at 12 nM, and the SARS-CoV-2 pseudo viral particles were tested at 10^5 vp/mL. Error bars are standard deviations, n = 3.

detection targets. In comparison with the SRBD, the SARS-CoV-2 viral particles feature multiple spike proteins (*i.e.,* 26) on their surfaces (Yao et al., 2020), thus allowing for detection signals to be further enhanced using a sandwich detection format (Huang et al., 2021). Since detection signals can be amplified using either a two-step amplification format (*i.e.,* conjugation of captured viral particles with RCA products that are subsequently hybridized with ssDNA-AuNPs) or a one-step amplification format (*i.e.,* conjugation of captured viral particles with RCA-AuNPs complex), both amplification strategies were tested and the amplified signals from the two methods were compared. As shown in Fig. 4A, the sensorgraph of the two-step format (*i.e.,* the black curve) showed a weak signal enhancement after the first step of signal amplification that involved RCA addition, with the signal intensified only by a factor of 1.7 (310 *vs.* 175 RU, see the black curve), an observation that was consistent with a previous study (He et al., 2014). However, the detection signal was significantly enhanced by approximately 6 times (1700 *vs.* 310 RU) after subsequent introduction of ssDNA-AuNPs. This is likely because a large number of ssDNA-AuNPs probes were hybridized with the RCA products, resulting in a significant enhancement of both the target mass and the plasmonic coupling effect (He et al., 2014; Kim et al., 2022). It should be noted that prolonging the RCA reaction time – thus the detection mass – to better increase the mass of targets did not work well (data not shown), as longer RCA reaction times resulted in visible white magnesium pyrophosphate precipitates that blocked the LSPR channels (Mori et al., 2001). In comparison, the one-step amplification format (see the red curve, Fig. 4A) exhibited no significant difference ($p>0.05$) in the final amplified signal when compared with the two-step amplification format (see the black curve). However, since the one-step amplification format required fewer injection steps (*i.e.,* 2 *vs.* 3 injections) and a shorter run time (500s *vs.* 800s), it was selected as the optimal signal intensification format for subsequent studies unless otherwise indicated.

To evaluate the detection performances of pseudo SARS-CoV-2 viral particles with RCA-AuNPs signal amplification, different concentrations of pseudo SARS-CoV-2 viral particles were detected using the (G3.5+G4)-aptamer modified sensor chips, followed by the signal amplification step using RCA-AuNPs. As shown in Fig. 4B, the sensorgraph presented low detection signals at any virus concentration before signal amplification was employed; in contrast, the detection signals were increased approximately 10-fold after the RCA-AuNPs complex was applied, indicating successful (and significant) detection signal intensification. Moreover, the LOD was calculated to be 148 vp/mL, one of the best sensitivities reported in whole viral particle detections amongst all detection platforms (Huang et al., 2021; Nguyen et al., 2016; Park et al., 2014; Yang et al., 2022). It should be noted that the typical SARS-CoV-2 viral concentration from nasopharyngeal and saliva swabbed samples is 10^4-10^{10} vp/mL (Huang et al., 2021), suggesting that the currently reported sensor chip modification and signal amplification approach can be readily used for early infection diagnostics to sensitively detect the SARS-CoV-2 virus. Moreover, the current approach directly detects whole viral particles; therefore, no sample pre-treatment would be required and the whole detection process can be done in 500 s, more efficient than any existing methods that require laborious sample preparations (Qiu et al., 2020; Yan et al., 2020). In addition, as shown in S4 (SI), the modified sensor chip can be regenerated multiple times using a regeneration solution (*i.e.,* glycine-HCL (10 mM, pH 2.0)), significantly saving the overall detection time and cost.

3.4. Detection specificity and influence of biological matrices

To study the specificity of (G3.5+G4)-aptamer sensor chip for detecting the SRBD samples, the target (*i.e.,* SARS-CoV-2 SRBD) and non-targets (*i.e.,* SARS-CoV SRBD and Middle East Respiratory Syndrome (MERS)-CoV SRBD) were tested. As shown in Fig. 5A (blue bars), signals for the target (*i.e.,* SARS-CoV-2 SRBD) were significantly higher than those of non-targets (*i.e.,* SARS-CoV SRBD and MERS-CoV SRBD), suggesting excellent detection specificity of the sensor chip for SARS-CoV-2 SRBD. To further study the specificity for pseudo viral particles detections, the SARS-CoV-2 pseudo viral particles (*i.e.,* targets) and negative pseudo viral particles with no spike protein on the surface (*i.e.,* non-targets) were detected using the (G3.5+G4)-aptamer sensor chip followed by signal amplification with RCA-AuNPs. As shown in Fig. 5A (yellow bars), the negative pseudo viral particles (*i.e.,* non-target) showed a low signal value at 23 RU compared to SARS-CoV-2 pseudo viral particles (*i.e.,* target) with a signal value at 970 RU, indicating an excellent detection specificity for SARS-CoV-2 pseudo viral particles. Moreover, the weak signal (7 RU) of the control sample (*i.e.,* Control = no viral particles) indicates minimal nonspecific interactions between the detection surface and the RCA-AuNPs. It is interesting to note that in comparison with a previously reported study in which RCA-AuNPs was also used to amplify SPR sensor chip detection signals (He et al., 2014), the background noises detected in the current study were much lower, further demonstrating the advantages of nonfouling properties of PAMAM dendrimers on the sensor chip detection surface design that also combines signal amplifications.

To investigate device performance under conditions that mimic real-world conditions, SARS-CoV-2 SRBD and SARS-CoV-2 pseudo viral particles were analyzed in PBS (pH 7.4), artificial saliva (1% v/v), and BSA (40 μg/mL) solutions (Lewis et al., 2021), as biological matrices are known to influence detection performances (Masson, 2020). As shown in Fig. 5B, in comparison with samples analyzed in PBS (pH 7.4), there was no significant ($p>0.05$) difference when either SRBD or pseudo viral particle samples were analyzed in saliva and BSA solutions. This is likely due to the nonfouling property of the modified detection surface, suggesting that the sensor chips proposed in this study were sufficiently

Table 1
Sensor-based LSPR system for detection of SARS-CoV-2 spike proteins and viral particles.

Biosensor technique	Target	Immobilized ligands	Sample matrix	LOD	Ref.
Polymer receptor functionalized plasmonic optical fibers	Spike protein subunit 1	Molecularly imprinted polymer receptor	Protein in buffer	58 nM	(Cennamo et al., 2021a)
Aptamer-PEG immobilized gold nanofilm-based optical fiber	SRBD	Aptamer against SRBD	Targets in diluted human serum	37 nM	(Cennamo et al., 2021b)
Streptavidin-aptamer immobilized LSPR sensor chip	Spike protein subunit 1	Aptamer against SRBD	S1 protein diluted in buffer	0.26 nM	(Lewis et al., 2021)
Antibody immobilized LSPR sensor chip with AuNPs signal amplification method	SARS-CoV-2 pseudovirus	Antibody against SRBD	Pseudovirus in buffer	370 vp/mL	(Huang et al., 2021)
ACE2 protein immobilized silver nanotriangle array	SRBD and Coronavirus	ACE2 protein	Buffer and Saliva	0.83 pM for SRBD, and 391 vp/mL for Coronavirus	(Yang et al., 2022)
Dendrimer-aptamer immobilized LSPR sensor chip	SRBD and SARS-CoV-2 pseudovirus	Aptamer against SRBD	Targets diluted in BSA and saliva	21.9 pM for SRBD, and 148 vp/mL for pseudovirus	This study

robust to reliably detect samples in complex biomatrices.

Table 1 compares the detection sensitivities achieved in the current report with those reported in recent literature. As can be seen in the table that the LODs achieved in this study for both targets (*i.e.,* SRBD and pseudovirus) were lower than most reported results. It is interesting to note that although the LOD for SRBD detection in this study was higher than the LOD reported by Yang et al., (2022) (*i.e.,* 21.9 pM *vs.* 0.83 pM), the LOD in this study for SARS-CoV-2 pseudovirus detections was lower (*i.e.,* 148 vp/mL *vs.* 391 vp/mL), potentially highlighting the added advantage of the RCA-AuNPs strategy for multiple signal amplification. In addition, unlike other conventional LSPR sensor chips designed for binding kinetic studies that aim for intermediate surface ligand densities to quickly reach binding equilibrium and to avoid mass transfer effects (Schasfoort, 2017), the current surface modification approach tries to maximize the surface ligand density to enhance detection sensitivities. As a result, the surface modification approach in combination with signal intensification strategies discussed in this study promise an interesting new direction for further exploration in order to expand the range of LSPR applications from what is conventionally only an analytical platform to a detection platform.

4. Conclusions

This study aims to improve the detection sensitivity of LSPR sensor chips to detect SARS-CoV-2 viral targets using a multi-pronged approach to both intensify detection signals and reduce background noises. To intensify the detection signals, three mechanisms have been employed: 1) surface immobilized PAMAM dendrimers as templates to introduce a large number of aptamers to the capturing sensor chip surfaces to enhance capturing probability and binding avidity for target recognition and capturing; 2) application of RCA to improve the target mass on the detection surface; and 3) use of AuNPs to increase both target mass and plasmonic coupling effect. To reduce the background noises, surface modification with two distinct PAMAM dendrimers that bind specifically to the different chip structures has been used to render the sensor chip surfaces nonfouling. Our results demonstrated that the modified sensor chips had a LOD of 21.9 pM for SRBD detection, approximately 152 times lower than that of the traditional antibody-based sensor chips. Our results also showed that the application of the RCA-AuNPs as the second-layer signal amplification further intensified detection signals by approximately 10 times and that the overall LOD was 148 vp/mL when used to detect pseudo SARS-CoV-2 viral particles, a sensitivity sufficiently high to suggest a potential application in early detection of COVID-19 infections. In addition, it is perceivable that the multi-pronged approach discussed in the current study can be readily adapted for other point-of-care applications based on already well-established LSPR/SPR detection platforms.

CRediT authorship contribution statement

Xingkai Hao: Conceptualization, Methodology, Validation, Formal analysis, Writing – original draft, Revision. **Jean-Philippe St-Pierre:** Writing – review & editing, Revision, Resources. **Shan Zou:** Investigation, Resources. **Xudong Cao:** Writing – review & editing, Revision, Supervision, Resources.

Declaration of competing interest

The authors declare that they have no known competing financial interests or personal relationships that could have appeared to influence the work reported in this paper.

Data availability

Data will be made available on request.

Acknowledgements

This work was supported by the Natural Sciences and Engineering Research Council of Canada (NSERC) Alliance COVID-19 Grants (ALLRP 550114-2020) and NSERC Discovery Grants (RGPIN-2018-06370) to XC. XH is supported by a scholarship from China Scholarship Council. We also thank Mr. Oltion Kodra from Energy, Mining and Environment Research Centre, National Research Council Canada, for the technical assistance with XPS analysis.

Appendix A. Supplementary data

Supplementary data to this article can be found online at https://doi.org/10.1016/j.bios.2023.115421.

References

Amouzadeh Tabrizi, M., Acedo, P., 2022. Appl. Surf. Sci. 598, 153867.
Cennamo, N., D'Agostino, G., Perri, C., Arcadio, F., Chiaretti, G., Parisio, E.M., Camarlinghi, G., Vettori, C., Di Marzo, F., Cennamo, R., 2021a. Sensors 21 (5), 1681.
Cennamo, N., Pasquardini, L., Arcadio, F., Lunelli, L., Vanzetti, L., Carafa, V., Altucci, L., Zeni, L., 2021b. Talanta 233, 122532.
De Feijter, J., Benjamins, d.J., Veer, F., 1978. Biopolymers: Original Research on Biomolecules 17 (7), 1759–1772.
Frens, G., 1973. Nat. Phys. Sci. (Lond.) 241 (105), 20–22.
Hao, X., Yang, X., Zou, S., Cao, X., 2023a. Appl. Surf. Sci. 610, 155603.
Hao, X., Yang, X., Zou, S., Cao, X., 2023b. Colloids Surf. B Biointerfaces 221, 113003.
He, P., Liu, L., Qiao, W., Zhang, S., 2014. Chem. Commun. 50 (12), 1481–1484.
Hermanson, G.T., 2013. Chapter 5 - homobifunctional crosslinkers. In: Hermanson, G.T. (Ed.), Bioconjugate Techniques, third ed. Academic Press, Boston, pp. 275–298.
Huang, L., Ding, L., Zhou, J., Chen, S., Chen, F., Zhao, C., Xu, J., Hu, W., Ji, J., Xu, H., 2021. Biosens. Bioelectron. 171, 112685.
Hurst, S.J., Lytton-Jean, A.K.R., Mirkin, C.A., 2006. Anal. Chem. 78 (24), 8313–8318.
Jiang, F., Xiao, Z., Wang, T., Wang, J., Bie, L., Saleh, L., Frey, K., Zhang, L., Wang, J., 2022. Chem. Commun. 58 (52), 7285–7288.
Jiang, Y., Li, S., Qiu, Z., Le, T., Zou, S., Cao, X., 2019. J. Food Saf. 39 (5), e12671.
Kim, H.-M., Kim, H.-J., Park, J.-H., Lee, S.-K., 2022. Anal. Chim. Acta 1213, 339960.
Lewis, T., Giroux, E., Jovic, M., Martic-Milne, S., 2021. Analyst 146 (23), 7207–7217.
Li, S., Jiang, Y., Yang, X., Lin, M., Dan, H., Zou, S., Cao, X., 2021. Anal. Chim. Acta 1150, 338229.
Lichtenberg, J.Y., Ling, Y., Kim, S., 2019. Sensors 19 (11), 2488.

Lu, M., Peng, W., Lin, M., Wang, F., Zhang, Y., 2021. Nanomaterials 11 (3), 616.
Masson, J.-F., 2020. ACS Sens. 5 (11), 3290–3292.
Mori, Y., Nagamine, K., Tomita, N., Notomi, T., 2001. Biochem. Biophys. Res. Commun. 289 (1), 150–154.
Nguyen, V.T., Seo, H.B., Kim, B.C., Kim, S.K., Song, C.S., Gu, M.B., 2016. Biosens. Bioelectron. 86, 293–300.
Park, J.-W., Jin Lee, S., Choi, E.-J., Kim, J., Song, J.-Y., Bock Gu, M., 2014. Biosens. Bioelectron. 51, 324–329.
Qiu, G., Gai, Z., Tao, Y., Schmitt, J., Kullak-Ublick, G.A., Wang, J., 2020. ACS Nano 14 (5), 5268–5277.
Raziq, A., Kidakova, A., Boroznjak, R., Reut, J., Öpik, A., Syritski, V., 2021. Biosens. Bioelectron. 178, 113029.
Samson, R., Navale, G.R., Dharne, M.S., 2020. 3 Biotech 10 (9), 385.
Schasfoort, R.B.M., 2017. Introduction to surface plasmon resonance. In: Schasfoort, R.B. M. (Ed.), Handbook of Surface Plasmon Resonance. The Royal Society of Chemistry, pp. 1–26.
Song, Y., Song, J., Wei, X., Huang, M., Sun, M., Zhu, L., Lin, B., Shen, H., Zhu, Z., Yang, C., 2020. Anal. Chem. 92 (14), 9895–9900.
Staros, J.V., 1982. Biochemistry 21 (17), 3950–3955.
Tian, B., Gao, F., Fock, J., Dufva, M., Hansen, M.F., 2020. Biosens. Bioelectron. 165, 112356.
Tuerk, C., Gold, L., 1990. Science 249 (4968), 505–510.
Unser, S., Bruzas, I., He, J., Sagle, L., 2015. Sensors 15 (7), 15684–15716.
Wang, Z., Yang, X., Lee, N.Z., Cao, X., 2022. Micromachines 13 (3), 436.
Xiang, Y., Deng, K., Xia, H., Yao, C., Chen, Q., Zhang, L., Liu, Z., Fu, W., 2013. Biosens. Bioelectron. 49, 442–449.
Xue, J., Li, Y., Liu, J., Zhang, Z., Yu, R., Huang, Y., Li, C., Chen, A., Qiu, J., 2022. Talanta 248, 123605.
Yan, C., Cui, J., Huang, L., Du, B., Chen, L., Xue, G., Li, S., Zhang, W., Zhao, L., Sun, Y., 2020. Clin. Microbiol. Infection 26 (6), 773–779.
Yang, Y., Murray, J., Haverstick, J., Tripp, R.A., Zhao, Y., 2022. Sensor. Actuator. B Chem. 359, 131604.
Yao, H., Song, Y., Chen, Y., Wu, N., Xu, J., Sun, C., Zhang, J., Weng, T., Zhang, Z., Wu, Z., Cheng, L., Shi, D., Lu, X., Lei, J., Crispin, M., Shi, Y., Li, L., Li, S., 2020. Cell 183 (3), 730–738 e713.
Zhao, Q., Duan, R., Yuan, J., Quan, Y., Yang, H., Xi, M., 2014. Int. J. Nanomed. 9, 1097.